

# Topological Waveguide Quantum Sensors

Tao Zhang,<sup>1</sup> Jiazhong Hu,<sup>1,2,\*</sup> and Xingze Qiu<sup>3,†</sup>

<sup>1</sup>Department of Physics and State Key Laboratory of Low Dimensional Quantum Physics, Tsinghua University, Beijing, 100084, China

<sup>2</sup>Frontier Science Center for Quantum Information and Collaborative Innovation Center of Quantum Matter, Beijing, 100084, China

<sup>3</sup>School of Physics Science and Engineering, Tongji University, Shanghai 200092, China

(Dated: November 3, 2023)

We present an efficient and robust protocol for quantum-enhanced sensing using a single-spin qubit in the topological waveguide system. Our method relies on the topological-paired bound states, which are localized near the spin and can be effectively regarded as a two-level system. Through the lens of Bayesian inference theory, we show the sensitivity can reach the Heisenberg limit across a large field range. Inheriting from the topological robustness of the waveguide, our sensing protocol is robust against local perturbations. The advantages of our protocol are multifold as it allows for sensing various parameters and uses a product initial state, which can be easily prepared in experiments. We expect this approach would pave the way towards robust topological quantum sensors based on near term quantum platforms such as topological photonics and Rydberg arrays.

*Introduction.*— Quantum sensing (QS) exploits quantum advantages for increasing the sensitivity of estimating certain physical parameters, and now represents a key technology in both fundamental science and concrete applications [1]. The sensitivity of QS can surpass the shot-noise limit (the best result of classical sensors) or even reach the Heisenberg limit, which is the limit on measurement precision imposed by quantum mechanics [2, 3]. Proposed applications of QS include magnetometry [4, 5], electrometry [6, 7], gravitational wave detection [8, 9], and dark matter detection [10].

Considerable efforts have been made to achieve quantum enhanced sensing, most of which focus on highly entangled Greenberger-Horne-Zeilinger (GHZ) [2, 3, 11] or N00N [12–14] states, spin-squeezed states [15, 16], and ground states of many-body systems at the critical point [17–21]. While these states have their own advantages, they also suffer from several obstacles, such as the experimental challenges in preparation and manipulation [22–25]. Therefore, other quantum sensing protocols have also been studied, and one area of particular interest is sensing with a single qubit [26–35]. These protocols have been realized in a variety of experimental platforms, including nitrogen-vacancy centers in diamond [26–29], rare-earth electron [33] and nuclear [34] spin qubit, photonic [30] and superconducting [32] qubit.

In this work, we introduce and characterize a novel protocol for sensing with a single qubit, which is inspired by the topological waveguide quantum electrodynamics (QED) setups [36–49]. These are systems where quantum emitters (QEs) couple to topological baths [see Fig. 1 (a) for example], which offers the opportunities to study emerging tailorable long-range interactions between QEs [37], topological physics with strongly interactions [50], and variational quantum simulators [51]. The key role is the two topological-paired bound states (BSs),

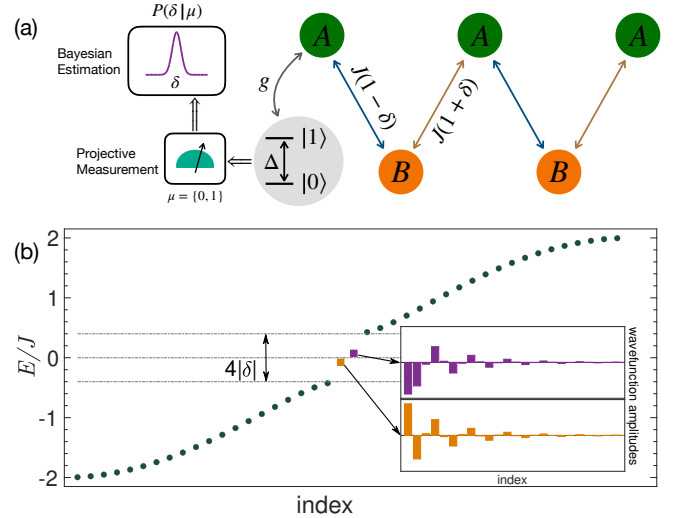


FIG. 1. (a) Schematic illustration of the topological waveguide quantum sensors. The SSH chain is characterized by having alternating hopping amplitudes  $J(1 \pm \delta)$  between sublattices  $A$  and  $B$ . A two-level QE with transition frequency  $\Delta$  couples to sublattice  $A$  at the leftmost site with a coupling strength  $g$ . The initial state of the system is a product state  $|\psi_0\rangle = |1\rangle \otimes |\text{vac}\rangle$ , i.e., the QE and the SSH chain lie in the excited state  $|1\rangle$  and the vacuum state  $|\text{vac}\rangle$ , respectively. After a sensing time, the state of the QE is measured, and the outcome  $\mu = \{0, 1\}$  is used to estimate the coupling strength  $g$  or the dimerization parameter  $\delta$  through Bayesian estimation. (b) Energy bands and BSs' properties. When QE's frequency is tuned to lie in the middle band gap with width  $4|\delta|$ , two exponentially localized BSs appear, whose energies and wavefunction amplitudes are shown by squares and bars, respectively. Here, we choose the transition frequency  $\Delta = 0$ , the coupling strength  $g = 0.1J$ , the dimerization parameter  $\delta = 0.2$ , and the system size  $N = 41$ .

which are localized around the QE when the QE's transition frequency lies deep in the middle band gap [52–54].

With this motivation, here we investigate the properties of a two-level QE coupled to a topological Su-Schrieffer-Heeger (SSH) waveguide. We find that when two BSs appear, the result of projective measurement on the QE can indeed be utilized for achieving quantum-enhanced sensitivity, and reach the Heisenberg limit with coherence time as quantum resource [55]. In addition, the sensitivity can be maintained across a large field range rather than the critical point. Moreover, inheriting from the bath's topological properties, our sensing protocol is robust to disorders, fluctuations of parameters, and other imperfections.

*Model.*— The system that we consider is shown in Fig. 1: A two-level QE interact with a SSH chain, which is characterized by having alternating hopping amplitudes  $J_{\pm} = J(1 \pm \delta)$  between two interspersed sublattice  $A$  and  $B$ . The QE couples to sublattice  $A$  at the leftmost site with a coupling strength  $g$ , and the transition frequency between the excited state  $|1\rangle$  and the ground state  $|0\rangle$  of the QE is  $\Delta$ . The total Hamiltonian of the system reads  $\hat{H} = \hat{H}_E + \hat{H}_S + \hat{H}_I$  with [37]

$$\hat{H}_E = \Delta \hat{\sigma}_+ \hat{\sigma}_-, \quad (1a)$$

$$\hat{H}_S = - \sum_{n=1}^{N-1} J_n (\hat{a}_n^\dagger \hat{a}_{n+1} + \text{H.c.}), \quad (1b)$$

$$\hat{H}_I = g (\hat{a}_1^\dagger \hat{\sigma}_- + \hat{a}_1 \hat{\sigma}_+). \quad (1c)$$

Here,  $N$  is the system size,  $J_n = J_- (J_+)$  for  $n$  odd (even),  $\hat{a}_n^\dagger$  ( $\hat{a}_n$ ) is the creation (annihilation) operator for a bosonic mode at the  $n$ -th site of the lattice, and  $\hat{\sigma}_- = (\hat{\sigma}_+)^{\dagger} = |0\rangle\langle 1|$  are the usual pseudospin ladder operators of the QE.

The Hamiltonian  $H_S$  in Eq. (1b) describes the topological SSH chain, and the physical consequences of the topological property are evidenced through the zero energy mode (ZEM) with open boundary conditions. Due to Lieb theorem [56], the dimerized SSH chain always has a ZEM for  $\forall \delta \neq 0$  if  $N$  is odd. Specifically, this ZEM will localize at the left (right) boundary if  $\delta > 0$  ( $\delta < 0$ ). At variance, for even  $N$ , no ZEM exist if  $\delta < 0$ , while two localized ZEMs will respectively appear at each end of the SSH chain if  $\delta > 0$ . Here, we find that the coupling of a QE to the SSH chain described by Eq. (1) gives rise to two localized BSs if the SSH bath chain has a ZEM localized near the QE and the QE's frequency is tuned to lie in the middle band gap of the bath dispersion [see Fig. 1 (b)]. This can be first qualitatively understood through degenerate perturbation theory if we set the frequency  $\Delta = 0$ : When the coupling strength  $g = 0$ , there are two degenerate zero energy states, i.e.,  $|\Phi_0\rangle = |0\rangle \otimes |\phi_0\rangle$  and  $|\Phi_1\rangle = |1\rangle \otimes |\phi_0\rangle$ , where  $|\phi_0\rangle$  denotes the ZEM of the SSH chain. With zero order approximation, these two states are corrected to be  $|\Phi_{B,\pm}\rangle = \frac{1}{\sqrt{2}} (|\Phi_0\rangle \pm |\Phi_1\rangle)$  if a weak coupling is turned on, and can thus be qualitatively viewed as the BSs. In fact, we can exactly solve the Schrödinger equation to obtain these BSs as shown

in the following.

Without loss of generality, we consider the resonance case  $\Delta = 0$  and the SSH chain with an odd number of sites that a ZEM exists at the leftmost site, i.e.,  $N$  is odd and  $\delta > 0$  [57]. For the two BSs  $|\Phi_{B,\pm}\rangle$  mentioned before, we can analytically obtain the corresponding eigenenergies  $E_{B,\pm} = \pm E_B$  and the overlap  $b_{\pm} = \langle \Phi_{B,\pm} | (|1\rangle \otimes |\text{vac}\rangle) \rangle = \mp b$ . Here,  $|\text{vac}\rangle$  denotes the vacuum state of the SSH chain,

$$E_B = g \sqrt{1 + \frac{J_-^2}{g^2 - J_+^2}}, \quad (2a)$$

$$b = \frac{1}{\sqrt{1 + \frac{1}{g^2(1-q^2)} \left[ E_B^2 + \left( \frac{g^2 - E_B^2}{J_-} \right)^2 \right]}}, \quad (2b)$$

with  $q = J_- J_+ / (g^2 - J_+^2)$ , and we have assumed  $|g| < 2J|\delta|$  such that the QE's frequency lies in the middle band gap [57]. In Fig. 1 (b), we plot the wavefunction amplitudes of the two BSs and their corresponding energies. We see that these two BSs are exponentially localized at the left boundary and have opposite energies, which are the key to our quantum enhanced sensing protocol as described below.

*Sensing precision bounds.*— Our goal is to achieve high discrimination of the coupling strength  $g$  or the dimerization parameter  $\delta$  by monitoring the dynamics of the topological waveguide QED system. Through the quantum dynamics, the information of  $g$  and  $\delta$  are transferred to the excitation population of QE which are subsequently read out [see Fig. 1 (a) for a pictorial illustration]. To be specific, we consider the unitary evolution  $|\psi(t)\rangle = \exp(-i\hat{H}t) |\psi(0)\rangle$  starting from an excited QE  $|\psi(0)\rangle = |1\rangle \otimes |\text{vac}\rangle$ , an initial state that can be easily prepared in experiments [38]. With the spectrum decomposition of the Hamiltonian  $\hat{H} = \sum_k E_k |\Phi_k\rangle\langle\Phi_k|$ , we have the survival amplitude of the initial state in the evolving state  $S(t) = \langle \psi(0) | \psi(t) \rangle = \sum_k |c_k|^2 \exp(-iE_k t)$ , where  $c_k = \langle \Phi_k | \psi(0) \rangle$ . Except for the two BSs  $|\Phi_{B,\pm}\rangle$ , the rest of the eigenstates of  $\hat{H}$  are extended bulk states, whose overlaps with the initial state can be safely ignored. Therefore, the survival amplitude  $S(t)$  can be well approximated by

$$\tilde{S}(t) = \sum_{\alpha=\pm} |\langle \Phi_{B,\alpha} | \psi(0) \rangle|^2 e^{-iE_{B,\alpha} t} = 2b^2 \cos(E_B t). \quad (3)$$

Consequently, the dynamics of this topological waveguide QED system can be intuitively understood as Rabi oscillations of a two-level system. However, a significant difference should be emphasized: The probability of finding the QE in the excited state in our problem is  $P_1(t) = |S(t)|^2$ , which can be precisely approximated by  $\tilde{P}_1(t) = |\tilde{S}(t)|^2 = 4b^4 \cos^2(E_B t)$  [see the right inset of Fig. 2 (a)]. Whereas, for a conventional Rabi oscillation model, the qubit will cycle between the eigenstates

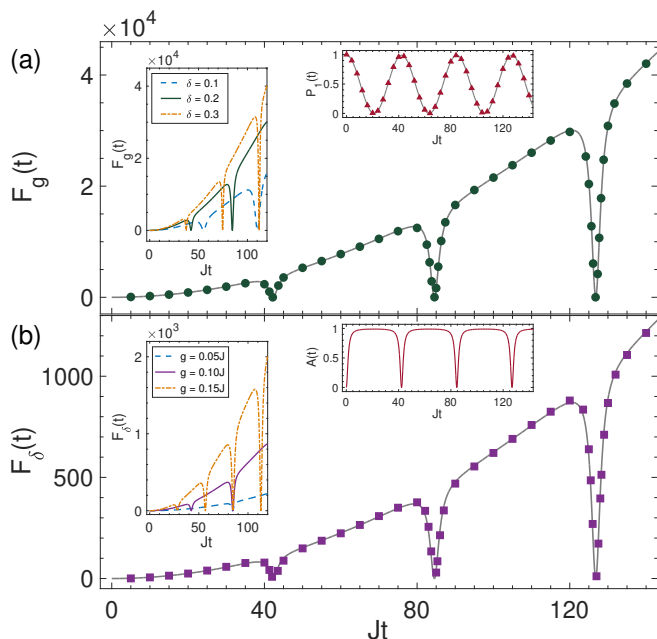


FIG. 2. Classical Fisher information (a)  $F_g(t)$  and (b)  $F_\delta(t)$  are plotted as green dots and purple squares, which can be precisely approximated by  $\tilde{F}_g(t)$  and  $\tilde{F}_\delta(t)$  (gray lines), respectively. In the right inset of (a), QE's excited state occupation probability  $P_1(t)$  is shown by red triangles, which can be well approximated by  $\tilde{P}_1(t)$  (gray line). The right inset of (b) shows the factor  $A(t)$  appeared in Eq. (4), which has periodical dips. Here, we choose the transition frequency  $\Delta = 0$ , the coupling strength  $g = 0.1J$ , the dimerization parameter  $\delta = 0.2$ , and the system size  $N = 201$ . Besides, the left insets of (a) and (b) show  $F_g(t)$  ( $g = 0.1J$ ) and  $F_\delta(t)$  ( $\delta = 0.2$ ) as functions of  $t$  for different  $\delta$  and  $g$ , respectively.

$|0_R\rangle$  and  $|1_R\rangle$ , which have the eigenenergies, say  $-E_B$  and  $E_B$ , respectively. With the qubit initially in the  $|1_R\rangle$  state, the occupation probability on that state is  $\bar{P}_1(t) = \cos^2(E_B t)$  [58]. This difference has direct consequences in the Fisher information as we explain in detail later.

The sensing precision for estimating an unknown parameter  $x$  is limited by the celebrated Cramér-Rao bound, i.e., the variance  $\text{Var}(x_{\text{est}}) \geq 1/F_x$ , where  $x_{\text{est}}$  is an estimator of  $x$  and  $F_x$  is Fisher information [59, 60]. Here, we estimate the coupling strength  $g$  or the dimerization parameter  $\delta$  through the measurement of the relative phase accumulated between the two states  $|0\rangle$  and  $|1\rangle$ , which is equivalent to measure the occupation probability  $P_1(t)$ . Therefore, the corresponding sensing bound is given by the classical Fisher information  $F_x(t) = [\partial P_1(t)/\partial x]^2 / (P_1(t)[1 - P_1(t)])$  [61], where  $x = g, \delta$ . Substituting  $P_1(t)$  by  $\tilde{P}_1(t)$  and keeping only the quadratic time dependent term,  $F_x(t)$  can be approximated by

$$\tilde{F}_x(t) = 4 \left( \frac{\partial E_B}{\partial x} \right)^2 A(t) t^2. \quad (4)$$

Here, the factor  $A(t) = 4b^4 \sin^2(E_B t) / [1 - 4b^4 \cos^2(E_B t)]$ , which is periodically time dependent as illustrated as the right inset of Fig. 2 (b). Therefore, both  $F_g(t)$  and  $F_\delta(t)$  are also modulated by the periodical time factor, which gives rise to the occurrence of periodical dips as exhibited in Fig. 2 (a) and (b), respectively. In contrast, the classical Fisher information corresponding to the Rabi oscillation model is  $\bar{F}_x(t) = [\partial \bar{P}_1(t)/\partial x]^2 / (\bar{P}_1(t)[1 - \bar{P}_1(t)]) = 4(\partial E_B/\partial x)^2 t^2$ , which is purely quadratic time dependent. But even with this difference, we will show in the following that our sensing protocol can achieve the Heisenberg limit with coherence time as quantum resource [55]. Note that the system size should be chosen as  $N \sim Jt$  such that this limit can be achieved [57].

In the left inset of Fig. 2 (a), we also show  $F_g(t)$  for different parameters  $\delta$ . We see that larger  $\delta$  can achieve higher Fisher information, since the corresponding BSs are more localized and thus more susceptible to the variation of the coupling strength  $g$ . However, this convenience comes at the cost that more frequent the occurrence of the dips. A similar phenomenon can be found for the parameter  $g$  dependence of  $F_\delta(t)$ , as illustrated in the left inset of Fig. 2 (b). These results give the guiding principle for choosing appropriate  $\delta$  and  $g$  to sense  $g$  and  $\delta$ , respectively.

*Bayesian parameter estimation.*— Here, we adopt Bayesian parameter estimators to saturate the Cramér-Rao bound [60, 62, 63], such that the sensing precision can achieve the Heisenberg limit mentioned before. The theory of estimation is based on the Bayes rule  $P(x|D) = P(D|x)P(x)/P(D)$ . Here, the posterior  $P(x|D)$  is the conditional probability of the parameter  $x$ , given the observed data  $D$ . The prior  $P(x)$  is the marginal probability of  $x$  accounting for the initial information about  $x$ . The prior is updated to the posterior through the likelihood  $P(D|x)$ , which imprints the measurement results. The denominator  $P(D)$  is the marginal probability of  $D$  accounting for a normalization factor such that  $\int dx P(x|D) = 1$ .

In our problem, we repeat the early mentioned preparation, evolution, and measurement procedure  $M$  times, and the probability of finding  $m$  outcomes at the excited state of the QE follows the binomial distribution and can be viewed as the likelihood

$$P(D|x) = \binom{M}{m} P_1^m(t) [1 - P_1(t)]^{M-m}. \quad (5)$$

Assuming the prior  $P(x)$  is a uniform distribution within some interval that we believe the unknown parameter  $x$  belongs to, the posterior is then  $P(x|D) \propto P(D|x)$ . As  $M$  becomes large,  $P(x|D)$  converges to a Gaussian centered at the true value of the unknown parameter  $x$  and with a width proportional to the square root of inverse Fisher information [64]. In order to quantify the uncertainty of estimation as well as the bias in the estimation,

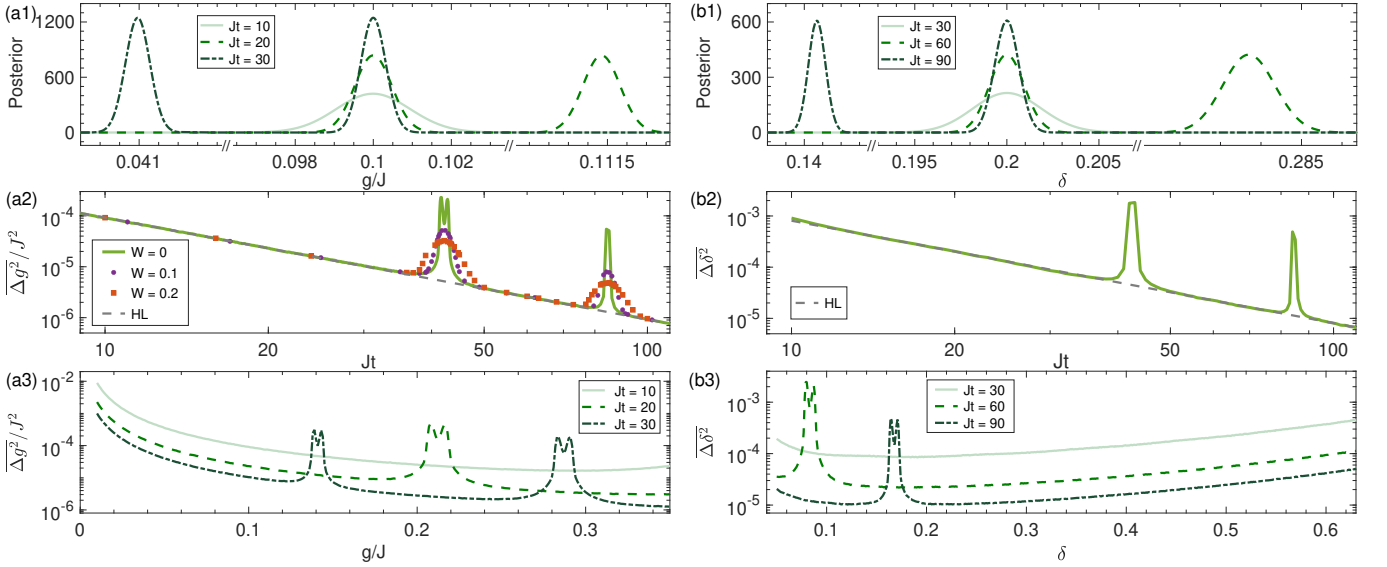


FIG. 3. Bayesian parameter estimation for (a) the coupling strength  $g$  and (b) the dimerization parameter  $\delta$ . (a1) and (b1), posterior distributions for three evolution time for sensing  $g = 0.1J$  and  $\delta = 0.2$  with uniform priors  $g \in [0, 0.2J]$  and  $\delta \in [0, 0.4]$ , respectively. The Gaussians centered at the true value become narrower by increasing the evolution time. (a2) and (b2), average of  $\Delta g^2$  and  $\Delta \delta^2$  (green solid lines) as functions of  $t$  for sensing  $g = 0.1J$  and  $\delta = 0.2$ , respectively. Both of them can achieve the Heisenberg limit (HL) indicated by the gray dashed lines. In (a2), the purple dots and red squares show the averaged  $\Delta g^2$  for disorder strength  $W = 0.1$  and  $W = 0.2$ , respectively. (a3) and (b3), average of  $\Delta g^2$  and  $\Delta \delta^2$  as functions of  $g$  and  $\delta$  for three evolution time, respectively. Here, we choose the transition frequency  $\Delta = 0$ , the system size  $N = 201$ , and for estimating  $g$  ( $\delta$ ), we have fixed  $\delta = 0.2$  ( $g = 0.1J$ ). In all of the plots, the posterior is obtained by repeating the sensing procedure for  $M = 10^4$  times, and each data point is averaged over  $N = 10^4$  samples.

we adopt the average squared relative error

$$\Delta x^2 = \frac{\sigma_x^2 + |\langle x \rangle - x|^2}{|x|^2}, \quad (6)$$

where  $\sigma_x^2$  and  $\langle x \rangle$  are the variance and the average of  $x$  with respect to the posterior  $P(x|D)$ , respectively. Note that  $\Delta x$  reduces to the inverse of the signal-to-noise ratio if the estimation is unbiased.

Fig. 3 shows our numerical results for estimating the coupling strength  $g$  and the dimerization parameter  $\delta$ . In Fig. 3 (a1), we plot the posterior as a function of  $g$  when the true value is  $g = 0.1J$  for different evolution time, where we have assumed a uniform prior  $g \in [0, 0.2J]$  and fixed the dimerization parameter as  $\delta = 0.2$ . We see that the Gaussian shapes centered at the true value become narrower by increasing the evolution time, indicating enhancement of the sensing precision. On the other hand, since the accumulated relative phase between the two states  $|0\rangle$  and  $|1\rangle$  has the freedom of modulo  $2\pi$ , some other Gaussian shapes can appear away from the true value. This ambiguity, however, can be solved by comparing measurements with slightly different evolution time. Our sensing protocol can indeed achieve the Heisenberg limit as shown in Fig. 3 (a2) (see the line corresponding to  $W = 0$  as explained below), where the average squared relative error  $\Delta g^2 \sim t^{-2}$  except for some peaks. We have checked that these peaks result from the

dips in the corresponding Fisher information, and can be easily avoided by chosen other evolution time. To further show the generality of our sensing protocol, in Fig. 3 (a3), we plot  $\Delta g^2$  over a broad range of  $g$  for different evolution time. Evidenced by the results, increasing coherence time can significantly enhance the sensing precision across a wide range of  $g$ , except for those regions around the peaks, which again result from the dips in the corresponding Fisher information as we have checked. Similar results can be found in Fig. 3 (b1-b3) for estimating the dimerization parameter  $\delta$ , where we have fixed the coupling strength as  $g = 0.1J$ .

Another remarkable property of our sensing protocol is the robustness to disorder. When the transition frequency  $\Delta = 0$ , our model Hamiltonian  $\hat{H}$  has chiral symmetry  $\hat{C}\hat{H}\hat{C} = -\hat{H}$  with  $\hat{C} = |1\rangle\langle 1| + \sum_{n=1}^N (-1)^n \hat{a}_n^\dagger \hat{a}_n$ . Inheriting from this, the BSs are robust to disorder and so it is when sensing the coupling strength  $g$ . To illustrate it, we study the effect of off-diagonal disorder, which appears in the hopping amplitudes between sublattices  $A$  and  $B$ , and preserves the chiral symmetry. In this case, the bath's Hamiltonian  $H_S \rightarrow H_S + J \sum_n (w_n \hat{a}_n^\dagger \hat{a}_{n+1} + \text{H.c.})$ , where we take the disorder  $w_n$  from a uniform distribution within the range  $[-W/2, W/2]$ . As shown in Fig. 3 (a2), the disorder diminishes and broadens the peaks of  $\Delta g^2$ . Other than that, it barely affects the precision in estimating  $g$  within a considerable range of



disorder strength. In addition, the dephasing effect has also been considered as shown in the Supplemental Material, where quantum-enhanced sensitivity can be achieved even when the dephasing rate is up to  $5\%J$ , which indicates that our sensing protocol is robust against such dephasing noise [57].

*Conclusion.*— We have devised a versatile and robust protocol for quantum sensing with the topological waveguide QED system, which can achieve the Heisenberg limit precision across a large field range. Through analytical investigation, we show the key of our protocol is the two paired BSs that inherit the topological robustness of the bath. Our sensing protocol thus paves the way for development of topological quantum sensors, which are expected to be robust against local perturbations. Besides, the single qubit based schemes demand simple projective measurement, thus may soon lead to experimental demonstrations of our protocol. Candidate near term quantum platforms including topological photonics [38] and Rydberg arrays [65].

This work is supported by National Key Research and Development Program of China (2021YFA0718303, 2021YFA1400904) and National Natural Science Foundation of China (92165203, 61975092, 11974202).

---

\* [hujiazhong01@ultracold.cn](mailto:hujiazhong01@ultracold.cn)

† [xingze@tongji.edu.cn](mailto:xingze@tongji.edu.cn)

- [1] C. L. Degen, F. Reinhard, and P. Cappellaro, Quantum sensing, *Rev. Mod. Phys.* **89**, 035002 (2017).
- [2] V. Giovannetti, S. Lloyd, and L. Maccone, Quantum-Enhanced Measurements: Beating the Standard Quantum Limit, *Science* **306**, 1330 (2004).
- [3] V. Giovannetti, S. Lloyd, and L. Maccone, Quantum Metrology, *Phys. Rev. Lett.* **96**, 010401 (2006).
- [4] J. M. Taylor, P. Cappellaro, L. Childress, L. Jiang, D. Budker, P. R. Hemmer, A. Yacoby, R. Walsworth, and M. D. Lukin, High-sensitivity diamond magnetometer with nanoscale resolution, *Nature Physics* **4**, 810 (2008).
- [5] T. Tanaka, P. Knott, Y. Matsuzaki, S. Dooley, H. Yamaguchi, W. J. Munro, and S. Saito, Proposed Robust Entanglement-Based Magnetic Field Sensor Beyond the Standard Quantum Limit, *Phys. Rev. Lett.* **115**, 170801 (2015).
- [6] F. Dolde, H. Fedder, M. W. Doherty, T. Nöbauer, F. Rempp, G. Balasubramanian, T. Wolf, F. Reinhard, L. C. L. Hollenberg, F. Jelezko, and J. Wrachtrup, Electric-field sensing using single diamond spins, *Nature Physics* **7**, 459 (2011).
- [7] A. Facon, E.-K. Dietsche, D. Grosso, S. Haroche, J.-M. Raimond, M. Brune, and S. Gleyzes, A sensitive electrometer based on a Rydberg atom in a Schrödinger-cat state, *Nature* **535**, 262 (2016).
- [8] C. M. Caves, Quantum-mechanical noise in an interferometer, *Phys. Rev. D* **23**, 1693 (1981).
- [9] M. Tse, H. Yu, and N. Kijbunchoo *et al.*, Quantum-Enhanced Advanced LIGO Detectors in the Era of Gravitational-Wave Astronomy, *Phys. Rev. Lett.* **123**, 231107 (2019).
- [10] S. Rajendran, N. Zobrist, A. O. Sushkov, R. Walsworth, and M. Lukin, A method for directional detection of dark matter using spectroscopy of crystal defects, *Phys. Rev. D* **96**, 035009 (2017).
- [11] F. Fröwis and W. Dür, Stable Macroscopic Quantum Superpositions, *Phys. Rev. Lett.* **106**, 110402 (2011).
- [12] J. P. Dowling, Quantum optical metrology – the low-down on high-N00N states, *Contemporary Physics* **49**, 125 (2008).
- [13] J. Joo, W. J. Munro, and T. P. Spiller, Quantum Metrology with Entangled Coherent States, *Phys. Rev. Lett.* **107**, 083601 (2011).
- [14] W. Chen, J. Hu, Y. Duan, B. Braverman, H. Zhang, and V. Vuletić, Carving Complex Many-Atom Entangled States by Single-Photon Detection, *Phys. Rev. Lett.* **115**, 250502 (2015).
- [15] D. J. Wineland, J. J. Bollinger, W. M. Itano, F. L. Moore, and D. J. Heinzen, Spin squeezing and reduced quantum noise in spectroscopy, *Phys. Rev. A* **46**, R6797 (1992).
- [16] M. Kitagawa and M. Ueda, Squeezed spin states, *Phys. Rev. A* **47**, 5138 (1993).
- [17] P. Zanardi, M. G. A. Paris, and L. Campos Venuti, Quantum criticality as a resource for quantum estimation, *Phys. Rev. A* **78**, 042105 (2008).
- [18] J. de Hond, J. Xiang, W. C. Chung, E. Cruz-Colón, W. Chen, W. C. Burton, C. J. Kennedy, and W. Ketterle, Preparation of the Spin-Mott State: A Spinful Mott Insulator of Repulsively Bound Pairs, *Phys. Rev. Lett.* **128**, 093401 (2022).
- [19] L. Liang, W. Zheng, R. Yao, Q. Zheng, Z. Yao, T.-G. Zhou, Q. Huang, Z. Zhang, J. Ye, X. Zhou, X. Chen, W. Chen, H. Zhai, and J. Hu, Probing quantum many-body correlations by universal ramping dynamics, *Science Bulletin* **67**, 2550 (2022).
- [20] L. Liang, Y. Wang, Q. Huang, Q. Zheng, X. Chen, and J. Hu, Probing quantum phase transition point by tuning an external anti trap, *Opt. Express* **31**, 16743 (2023).
- [21] W. C. Burton, C. J. Kennedy, W. C. Chung, S. Vadia, W. Chen, and W. Ketterle, Coherence Times of Bose-Einstein Condensates beyond the Shot-Noise Limit via Superfluid Shielding, *Phys. Rev. Lett.* **117**, 275301 (2016).
- [22] R. Demkowicz-Dobrzański, J. Kołodyński, and M. Guţă, The elusive Heisenberg limit in quantum-enhanced metrology, *Nature Communications* **3**, 1063 (2012).
- [23] M. M. Rams, P. Sierant, O. Dutta, P. Horodecki, and J. Zakrzewski, At the Limits of Criticality-Based Quantum Metrology: Apparent Super-Heisenberg Scaling Revisited, *Phys. Rev. X* **8**, 021022 (2018).
- [24] Y. Zhao, R. Zhang, and W. Chen, Creation of Greenberger-Horne-Zeilinger states with thousands of atoms by entanglement amplification, *npj Quantum Information* **7**, 24 (2021).
- [25] R. McConnell, H. Zhang, J. Hu, S. Čuk, and V. Vuletić, Entanglement with negative Wigner function of almost 3,000 atoms heralded by one photon, *Nature* **519**, 439 (2015).
- [26] S. Kolkowitz, A. C. Bleszynski Jayich, Q. P. Unterreithmeier, S. D. Bennett, P. Rabl, J. G. E. Harris, and M. D. Lukin, Coherent Sensing of a Mechanical Resonator with

- a Single-Spin Qubit, *Science* **335**, 1603 (2012).
- [27] H. J. Mamin, M. Kim, M. H. Sherwood, C. T. Rettner, K. Ohno, D. D. Awschalom, and D. Rugar, Nanoscale Nuclear Magnetic Resonance with a Nitrogen-Vacancy Spin Sensor, *Science* **339**, 557 (2013).
- [28] S. Kolkowitz, A. Safira, A. A. High, R. C. Devlin, S. Choi, Q. P. Unterreithmeier, D. Patterson, A. S. Zibrov, V. E. Manucharyan, H. Park, and M. D. Lukin, Probing Johnson noise and ballistic transport in normal metals with a single-spin qubit, *Science* **347**, 1129 (2015).
- [29] C. Bonato, M. S. Blok, H. T. Dinani, D. W. Berry, M. L. Markham, D. J. Twitchen, and R. Hanson, Optimized quantum sensing with a single electron spin using real-time adaptive measurements, *Nature Nanotechnology* **11**, 247 (2016).
- [30] S. Clemmen, A. Farsi, S. Ramelow, and A. L. Gaeta, Ramsey Interference with Single Photons, *Phys. Rev. Lett.* **117**, 223601 (2016).
- [31] F. Poggiali, P. Cappellaro, and N. Fabbri, Optimal Control for One-Qubit Quantum Sensing, *Phys. Rev. X* **8**, 021059 (2018).
- [32] D. Lachance-Quirion, S. P. Wolski, Y. Tabuchi, S. Kono, K. Usami, and Y. Nakamura, Entanglement-based single-shot detection of a single magnon with a superconducting qubit, *Science* **367**, 425 (2020).
- [33] T. Kornher, D.-W. Xiao, K. Xia, F. Sardi, N. Zhao, R. Kolesov, and J. Wrachtrup, Sensing Individual Nuclear Spins with a Single Rare-Earth Electron Spin, *Phys. Rev. Lett.* **124**, 170402 (2020).
- [34] D. M. Jackson, D. A. Gangloff, J. H. Bodey, L. Zaporski, C. Bachorz, E. Clarke, M. Hugues, C. Le Gall, and M. Atatüre, Quantum sensing of a coherent single spin excitation in a nuclear ensemble, *Nature Physics* **17**, 585 (2021).
- [35] G. Wang, Y.-X. Liu, J. M. Schloss, S. T. Alsid, D. A. Braje, and P. Cappellaro, Sensing of Arbitrary-Frequency Fields Using a Quantum Mixer, *Phys. Rev. X* **12**, 021061 (2022).
- [36] S. Barik, A. Karasahin, C. Flower, T. Cai, H. Miyake, W. DeGottardi, M. Hafezi, and E. Waks, A topological quantum optics interface, *Science* **359**, 666 (2018).
- [37] M. Bello, G. Platero, J. I. Cirac, and A. González-Tudela, Unconventional quantum optics in topological waveguide QED, *Science Advances* **5**, eaaw0297 (2019).
- [38] E. Kim, X. Zhang, V. S. Ferreira, J. Banker, J. K. Iverson, A. Sipahigil, M. Bello, A. González-Tudela, M. Mirhosseini, and O. Painter, Quantum Electrodynamics in a Topological Waveguide, *Phys. Rev. X* **11**, 011015 (2021).
- [39] L. Leonforte, A. Carollo, and F. Ciccarello, Vacancy-like Dressed States in Topological Waveguide QED, *Phys. Rev. Lett.* **126**, 063601 (2021).
- [40] D. De Bernardis, Z.-P. Cian, I. Carusotto, M. Hafezi, and P. Rabl, Light-Matter Interactions in Synthetic Magnetic Fields: Landau-Photon Polaritons, *Phys. Rev. Lett.* **126**, 103603 (2021).
- [41] C. Vega, M. Bello, D. Porras, and A. González-Tudela, Qubit-photon bound states in topological waveguides with long-range hoppings, *Phys. Rev. A* **104**, 053522 (2021).
- [42] Z. Gong, M. Bello, D. Malz, and F. K. Kunst, Anomalous Behaviors of Quantum Emitters in Non-Hermitian Baths, *Phys. Rev. Lett.* **129**, 223601 (2022).
- [43] W. Cheng, Z. Wang, and Y.-x. Liu, Topology and retardation effect of a giant atom in a topological waveguide, *Phys. Rev. A* **106**, 033522 (2022).
- [44] M. Bello, G. Platero, and A. González-Tudela, Spin Many-Body Phases in Standard- and Topological-Waveguide QED Simulators, *PRX Quantum* **3**, 010336 (2022).
- [45] C. Vega, D. Porras, and A. González-Tudela, Topological multimode waveguide QED, *Phys. Rev. Res.* **5**, 023031 (2023).
- [46] M. Bello and J. I. Cirac, Topological effects in two-dimensional quantum emitter systems, *Phys. Rev. B* **107**, 054301 (2023).
- [47] C. I. Kvand, D. B. Hill, and D. Blume, Finite Su-Schrieffer-Heeger chains coupled to a two-level emitter: Hybridization of edge and emitter states, *Phys. Rev. A* **108**, 023703 (2023).
- [48] A. S. Sheremet, M. I. Petrov, I. V. Iorsh, A. V. Poshakinskiy, and A. N. Poddubny, Waveguide quantum electrodynamics: Collective radiance and photon-photon correlations, *Rev. Mod. Phys.* **95**, 015002 (2023).
- [49] C. Joshi, F. Yang, and M. Mirhosseini, Resonance Fluorescence of a Chiral Artificial Atom, *Phys. Rev. X* **13**, 021039 (2023).
- [50] B. M. Anderson, R. Ma, C. Owens, D. I. Schuster, and J. Simon, Engineering Topological Many-Body Materials in Microwave Cavity Arrays, *Phys. Rev. X* **6**, 041043 (2016).
- [51] C. Tabares, A. Muñoz de las Heras, L. Tagliacozzo, D. Porras, and A. González-Tudela, Variational Quantum Simulators Based on Waveguide QED, *Phys. Rev. Lett.* **131**, 073602 (2023).
- [52] V. P. Bykov, Spontaneous emission from a medium with a band spectrum, *Soviet Journal of Quantum Electronics* **4**, 861 (1975).
- [53] S. John and J. Wang, Quantum electrodynamics near a photonic band gap: Photon bound states and dressed atoms, *Phys. Rev. Lett.* **64**, 2418 (1990).
- [54] G. Kurizki, Two-atom resonant radiative coupling in photonic band structures, *Phys. Rev. A* **42**, 2915 (1990).
- [55] D. Braun, G. Adesso, F. Benatti, R. Floreanini, U. Marzolino, M. W. Mitchell, and S. Pirandola, Quantum-enhanced measurements without entanglement, *Rev. Mod. Phys.* **90**, 035006 (2018).
- [56] E. H. Lieb, Two theorems on the Hubbard model, *Phys. Rev. Lett.* **62**, 1201 (1989).
- [57] See Supplemental Materials for technical details and extended derivations.
- [58] J. Garrison and R. Chiao, *Quantum Optics* (Oxford University Press, 2008).
- [59] C. R. Rao, Information and the Accuracy Attainable in the Estimation of Statistical Parameters, in *Breakthroughs in Statistics: Foundations and Basic Theory*, edited by S. Kotz and N. L. Johnson (Springer New York, New York, NY, 1992) pp. 235–247.
- [60] H. Cramér, *Mathematical Methods of Statistics (PMS-9)* (Princeton University Press, 1999).
- [61] L. Pezzè, A. Smerzi, M. K. Oberthaler, R. Schmied, and P. Treutlein, Quantum metrology with nonclassical states of atomic ensembles, *Rev. Mod. Phys.* **90**, 035005 (2018).
- [62] Z. Hradil, R. Myška, J. Peřina, M. Zawisky, Y. Hasegawa, and H. Rauch, Quantum Phase in Interferometry, *Phys. Rev. Lett.* **76**, 4295 (1996).
- [63] L. Pezzè, A. Smerzi, G. Khoury, J. F. Hodelin, and D. Bouwmeester, Phase Detection at the Quantum Limit

- with Multiphoton Mach-Zehnder Interferometry, *Phys. Rev. Lett.* **99**, 223602 (2007).
- [64] E. L. Lehmann and G. Casella, *Theory of Point Estimation* (Springer New York, NY, 1998).
- [65] S. de Léséleuc, V. Lienhard, P. Scholl, D. Barredo, S. Weber, N. Lang, H. P. Büchler, T. Lahaye, and A. Browaeys, Observation of a symmetry-protected topological phase of interacting bosons with Rydberg atoms, *Science* **365**, 775 (2019).

# Supplementary Material: Topological Waveguide Quantum Sensors

Tao Zhang,<sup>1</sup> Jiazhong Hu,<sup>1,2,\*</sup> and Xingze Qiu<sup>3,†</sup>

<sup>1</sup>*Department of Physics and State Key Laboratory of Low Dimensional  
Quantum Physics, Tsinghua University, Beijing, 100084, China*

<sup>2</sup>*Frontier Science Center for Quantum Information and Collaborative  
Innovation Center of Quantum Matter, Beijing, 100084, China*

<sup>3</sup>*School of Physics Science and Engineering, Tongji University, Shanghai 200092, China*

(Dated: November 3, 2023)

The present supplemental material provides more details about our sensing protocol, including analytical solution for the bound states, the applicability of our sensing protocol for even system size, the finite size effect, and the robustness of our protocol against dephasing.

## CONTENTS

Analytical Solutions for the Bound States	2
Applicability of our sensing protocol for even system size	2
Finite Size Effect	3
Sensing in the presence of dephasing	4
References	5



## ANALYTICAL SOLUTIONS FOR THE BOUND STATES

The model Hamiltonian we considered in the main text reads  $\hat{H} = \hat{H}_E + \hat{H}_S + \hat{H}_I$  with

$$\hat{H}_E = \Delta \hat{\sigma}_+ \hat{\sigma}_-, \quad (\text{S-1a})$$

$$\hat{H}_S = - \sum_{n=1}^{N-1} J_n (\hat{a}_n^\dagger \hat{a}_{n+1} + \text{H.c.}), \quad (\text{S-1b})$$

$$\hat{H}_I = g (\hat{a}_1^\dagger \hat{\sigma}_- + \hat{a}_1 \hat{\sigma}_+). \quad (\text{S-1c})$$

Here,  $J_n = J_-$  ( $J_+$ ) for  $n$  odd (even) with  $J_\pm = J(1 \pm \delta)$ ,  $N$  is the system size,  $\hat{a}_n^\dagger$  ( $\hat{a}_n$ ) is the creation (annihilation) operator for a bosonic mode at the  $n$ -th site of the lattice, and  $\hat{\sigma}_- = (\hat{\sigma}_+)^{\dagger} = |0\rangle\langle 1|$  are the usual pseudospin ladder operators of the quantum emitter (QE), which is located at the  $n = 1$  site. When a zero energy mode (ZEM) of the SSH chain existed at the left boundary, two bound states (BSs) will appear due to the coupling between the QE and the SSH chain, which can be showed as follows. In fact, the wave functions of these two BSs can be parametered as

$$|\Phi_B\rangle = \left( b \hat{\sigma}_+ + \sum_{n=1}^N c_n a_n^\dagger \right) (|0\rangle \otimes |\text{vac}\rangle). \quad (\text{S-2})$$

Here,  $b$  and  $c_n$  are real coefficients to be determined, and  $|\text{vac}\rangle$  denotes the vacuum state of the SSH chain. Without loss of generality, we assume  $0 < \delta < 1$  and  $N$  is odd, such that a ZEM localized at the left boundary. In order to obtain analytical solutions of the BSs, we adopt the Siegert boundary conditions with outgoing waves in the form [1, 2]

$$\begin{pmatrix} c_n \\ c_{n+1} \end{pmatrix} = \exp\left(ik \frac{n+1}{2}\right) \begin{pmatrix} d_1 \\ d_2 \end{pmatrix}, \quad \text{for odd } n, \quad (\text{S-3})$$

where the wave number  $k$  is a complex number for the BSs. Solving the Schrödinger equation  $\hat{H} |\Phi_B\rangle = E_B |\Phi_B\rangle$  with eigenvalue  $E_B$  and eigenstate  $|\Psi_b\rangle$  yields a series of coupled equations as follows

$$g d_1 = (E_B - \Delta) b e^{-ik}, \quad (\text{S-4a})$$

$$g b = (E_B d_1 + J_- d_2) e^{ik}, \quad (\text{S-4b})$$

$$E_B d_2 = -(J_- + J_+ e^{ik}) d_1, \quad (\text{S-4c})$$

$$E_B d_1 = -(J_- + J_+ e^{-ik}) d_2. \quad (\text{S-4d})$$

Together with the normalization condition  $b^2 + \sum_{n=1}^N c_n^2 = 1$  and the resonance condition  $\Delta = 0$ , we can obtain

$$E_B = \pm g \sqrt{1 + \frac{J_-^2}{g^2 - J_+^2}}, \quad (\text{S-5a})$$

$$b = \mp \left( 1 + \frac{1}{g^2(1-q^2)} \left[ E_B^2 + \left( \frac{g^2 - E_B^2}{J_-} \right)^2 \right] \right)^{-1/2}, \quad (\text{S-5b})$$

$$d_1 = \frac{1}{qg} E_B b, \quad (\text{S-5c})$$

$$d_2 = \frac{1}{qg} \frac{g^2 - E_B^2}{J_-} b, \quad (\text{S-5d})$$

$$e^{ik} = q, \quad (\text{S-5e})$$

where  $q = J_- J_+ / (g^2 - J_+^2)$ , and we have assumed the system size  $N$  is large enough and  $|g| < 2J|\delta|$ . By substituting Eq. (S-5) into Eq. (S-3) and then Eq. (S-2), we get the analytical solutions of the wave functions  $|\Phi_B\rangle$  of the two BSs, which have energies  $E_B$ . Since  $|q| < 1$ , these two BSs are exponentially localized at the left boundary.

## APPLICABILITY OF OUR SENSING PROTOCOL FOR EVEN SYSTEM SIZE

As has been discussed in the main text, the number of ZEM in a finite-size SSH chain depends on the parity of system size  $N$  and the sign of  $\delta$ . In the main text, we have discussed the situation of odd  $N$  and positive  $\delta$ . For

odd  $N$  and negative  $\delta$  case, our sensing protocol is still applicable by coupling the QE to the right end of the chain. Here, we numerically discuss the situation of even  $N$  and positive  $\delta$ , and in this case there are two localized ZEMs respectively appearing at each end of the SSH chain. As shown in Fig. S-1 (a), when a QE couples to the SSH chain, two topological-paired BSs near the QE appear. Besides, there is a ZEM localized at the right end of the chain. However, as illustrated in Fig. S-1 (b), this ZEM does not effect the sensing precision since it is far away from the BSs and thus has no effect to the dynamics of the BSs.

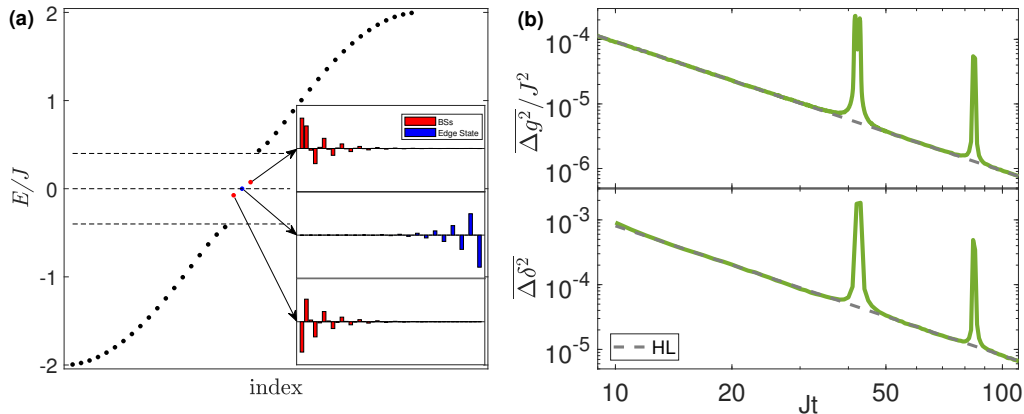


FIG. S-1. (a) Energy bands, topological-paired BSs, and ZEM. The inset shows wave function amplitudes of the BSs (top and bottom) and the ZEM (middle), respectively. Here, we choose the parameters  $N = 40$ ,  $\delta = 0.2$  and  $g = 0.1J$ . (b) Average squared relative errors of Bayesian parameter estimation for the coupling strength  $g$  and the dimerization parameter  $\delta$ . Here, for sensing  $g = 0.1J$  ( $\delta = 0.2$ ), we have fixed  $\delta = 0.2$  ( $g = 0.1J$ ). The system size and the transition frequency are chosen as  $N = 200$  and  $\Delta = 0$ , respectively. For both panels, the posterior is obtained by repeating the sensing procedure for  $M = 10^4$  times, and each data point is averaged over  $10^2$  samples. The grey dashed lines indicate the Heisenberg limit.

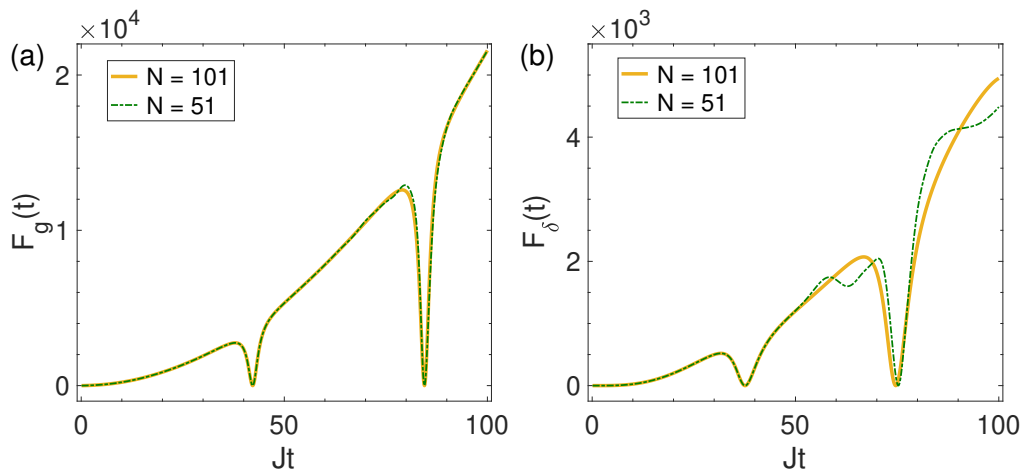


FIG. S-2. Classical Fisher information (a)  $F_g(t)$  and (b)  $F_\delta(t)$  as a function of coherence time  $t$  for different system sizes. Here, we choose the transition frequency  $\Delta = 0$ , the dimerization parameter  $\delta = 0.2$ , and the coupling strength  $g = 0.1J$ .

### FINITE SIZE EFFECT

Here, we give more discussion about the requirement that the system size should be chosen as  $N \sim Jt$ . In spite of very large overlap between the two topological-paired BSs and the initial state, the overlap between the bulk states and the initial state cannot be completely ignored. This faintest leakage will spread away from the QE and be rebounded by the other end of the SSH chain, and then propagate back towards the QE. The total time of this process can be reasonably assumed to be proportionate to the system size  $N$ . After this evolution time, the leakage can significantly

affect the dynamics of the two-level system formed by the two BSs. This affection is thus named as “finite size effect”. As shown in Fig. S-2, this effect can be directly observed through the classical Fisher information. We see that the Fisher information will oscillate when the evolution time  $Jt$  is larger than the system size  $N$ . In addition, compared with  $F_g(t)$ ,  $F_\delta(t)$  is more susceptible to the finite size effect.

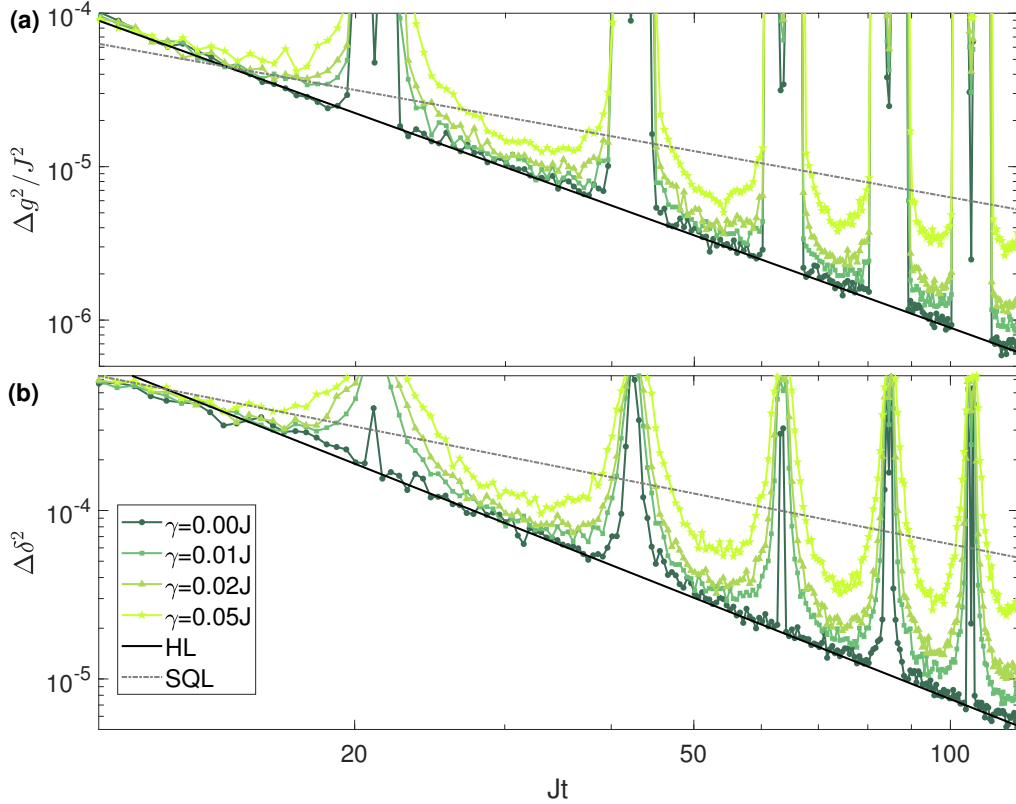


FIG. S-3. Average squared relative errors of Bayesian parameter estimation for (a) the coupling strength  $g$  and (b) the dimerization parameter  $\delta$ . Here, for sensing  $g = 0.1J$  ( $\delta = 0.2$ ), we have fixed  $\delta = 0.2$  ( $g = 0.1J$ ). The system size and the transition frequency are chosen as  $N = 201$  and  $\Delta = 0$ , respectively. For both panels, the posterior is obtained by repeating the sensing procedure for  $M = 10^4$  times, and each data point is averaged over  $10^2$  samples. Besides, we also show the standard quantum limit and Heisenberg limit in both panels.

### SENSING IN THE PRESENCE OF DEPHASING

In this section, we consider the dephasing effect, which is unavoidable in real scenarios. The quantum dynamics of our system is now undergoing a dephasing process for the QE with a constant rate  $\gamma$ , and governed by the following master equation

$$\dot{\rho}(t) = -i[H, \rho(t)] + \gamma \left( |1\rangle\langle 1| \rho(t) |1\rangle\langle 1| - \frac{1}{2} \{ |1\rangle\langle 1|, \rho(t) \} \right), \quad (\text{S-6})$$

where  $\rho$  is the system’s density matrix. Now the probability of finding the QE in the excited state is  $P_1'(t) = \text{Tr}(\rho(t) |1\rangle\langle 1|)$ , and we thus can sense the coupling strength  $g$  and the dimerization parameter  $\delta$  with the Bayesian parameter estimation method as shown in the main text. Our numerical results are shown in Fig. S-3, and we see that as the dephasing rate  $\gamma$  increases, the sensing precision for both  $g$  and  $\delta$  become worse. However, the quantum-enhanced sensitivity can still be achieved even when the dephasing rate is up to  $\gamma \sim 5\%J$ , which indicates that our sensing protocol is robust against such dephasing noise.

---

\* [hujiazhong01@ultracold.cn](mailto:hujiazhong01@ultracold.cn)

† [xingze@tongji.edu.cn](mailto:xingze@tongji.edu.cn)

- [1] N. Hatano, K. Sasada, H. Nakamura, and T. Petrosky, Some Properties of the Resonant State in Quantum Mechanics and Its Computation, *Progress of Theoretical Physics* **119**, 187 (2008).
- [2] N. Hatano, Equivalence of the effective Hamiltonian approach and the Siegert boundary condition for resonant states, *Fortschritte der Physik* **61**, 238 (2013).